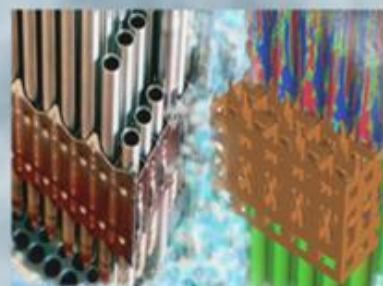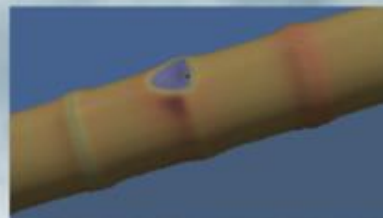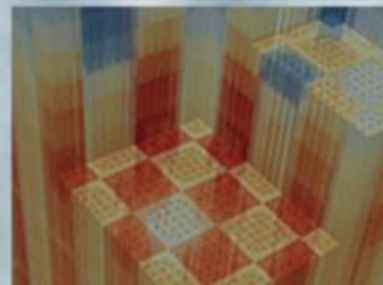# Validation of CTF Droplet Entrainment and Annular/Mist Closure Models using Riso Steam/Water Experiments

Aaron Wysocki, Oak Ridge National Laboratory
Robert Salko, Oak Ridge National Laboratory

04/29/2016

REVISION LOG

Revision	Date	Affected Pages	Revision Description
0	04/29/2016	All	Initial Release

Document pages that are:

Export Controlled _____

IP/Proprietary/NDA
Controlled_____

Sensitive Controlled_____

Unlimited_____All_____

Requested Distribution:

To: CASL-SLT

Copy: Kevin Clarno, Jeff Banta

EXECUTIVE SUMMARY

This report summarizes the work to validate the droplet entrainment and de-entrainment models, as well as two-phase closure models in the CTF code (an updated version of COBRA-TF) by comparison with experimental data obtained at Riso National Laboratory. The Riso data included a series of more than 250 steam/water experiments that were performed in both tube and annulus geometries over a range of various pressures and outlet qualities. Experimental conditions were set so that the majority of cases were in the annular/mist flow regime. Measurements included liquid film flow rate, droplet flow rate, film thickness, and two-phase pressure drop.

CTF was used to model 180 of the tubular geometry cases, matching experimental geometry, outlet pressure, and outlet flow quality to experimental values. CTF results were compared to the experimental data at the outlet of the test section in terms of vapor and entrained liquid flow fractions, pressure drop per unit length, and liquid film thickness. The entire process of generating CTF input decks, running cases, extracting data, and generating comparison plots was scripted using Python and Matplotlib for a completely automated validation process. All test cases and scripting tools have been committed to the COBRA-TF master repository, and selected cases have been added to the continuous testing system to serve as regression tests.

The differences between the CTF- and experimentally-calculated flow fraction values were consistent with previous calculations by Wurtz, who applied the same entrainment correlation to the same data. It has been found that CTF's entrainment/de-entrainment predictive capability in the annular/mist flow regime for this particular facility is comparable to the licensed industry code, CO-BRAG. Although film and droplet predictions are generally good, it has been found that accuracy diminishes at lower flow qualities. This finding is consistent with the noted deficiencies in the Wurtz entrainment model employed by CTF.

The CTF-predicted two-phase pressure drop in the annular/mist flow regime has been found to be highly inaccurate, exhibiting a clear bias with respect to the experimental data. This inaccuracy led to an investigation that revealed deficiencies in the implementation of the annular/mist interfacial friction model, which should be investigated further. Published COBRAG results for this same facility reveal that COBRAG exhibits no bias with regard to experimental pressure drop results. In addition to the problems with pressure drop prediction, the film thickness was also significantly under-predicted by CTF when compared to both experimental data and Wurtz's analytical calculations. Film thickness is calculated using a simple geometric relationship and film void fraction in CTF, which is dependent on the slip ratio and interfacial friction. It is possible that the issues affecting the pressure drop and film void prediction are related.

(This page intentionally left blank)

CONTENTS

FIGURES

TABLES

ACRONYMS

RMS root-mean-square

RMSE root-mean-square error

1 INTRODUCTION

1.1 Facility Description

Riso Report No. 372 describes the Riso experimental facility and associated tests [1]. In total, more than 250 tests were performed in four different types of geometries: (1)a 9 m long, 10 mm vertical tube; (2) a 9 m long, 20 mm vertical tube; (3) a 3.5 m long vertical annulus with a 17 mm inner diameter and a 26 mm outer diameter; and (4) an 8 m long vertical annulus with a 17 mm inner diameter and a 26 mm outer diameter. The range of geometric and operating conditions are shown in Table 1. These tests involve upward flow through a vertical cylindrical stainless steel pipe, either unheated or with a constant applied heat flux over a specified section of the pipe. Of these cases, seventy-eight were diabatic (i.e., with a heated test section) and the remaining 102 were adiabatic (i.e., the fluid was heated before it entered the test section to achieve a desired constant thermodynamic quality throughout the test section).

Film flow rates were measured by opening a bypass valve, which allowed the flow to be diverted through perforations in the pipe wall near the test section outlet. A heat balance unit was then used to measure the flow rate of liquid in the diverted flow, with a procedure to correct for any entrained droplet flow that may have been diverted as well. Although the heat balance units have a quantifiable amount of measurement uncertainty, the data correction procedure, on the other hand, has an unspecified and unknown level of uncertainty. Entrained droplet flow rates were calculated from the measured total flow rate, equilibrium quality, and film flow rate for each case. Pressure drops were measured via differential pressure cells across two locations: the last 1 m and the last 4 m of the test section.

Film thicknesses were measured with a needle contact probe inserted into the flow, with film thickness inferred from liquid contact time with the needle at various distances from the wall. Film and droplet flow rate measurements were available for all test points, whereas pressure drop data were only available for 102 of the adiabatic test points, and film thickness data were only available for 21 of the adiabatic test points.

1.2 CTF Modeling Approach

Datasets used for this study included 180 test points from the two tubular geometry test sections. A script was used to generate the CTF input files automatically for all test points. The CTF models were created using internal flow in a single channel, with the inlet flow rate and outlet pressure for each test point used as boundary conditions. Neither inlet enthalpy nor temperature were provided for the experiments; however, outlet quality for each case was specified, so the inlet enthalpy was calculated based on the total flow rate, total heat rate, and outlet quality for each case. Using the inferred inlet enthalpy values, the resulting outlet quality calculated by CTF matched the intended value from the experiment within an absolute difference of 1.0 % quality in each case, as shown in Figure 1. Note that the measurement uncertainty for outlet quality was 0.5 % (absolute), so improving the agreement in outlet quality below the level of uncertainty could be worthwhile for improving future results.

Table 1. Ranges of Operating Conditions for the Riso Test Points

Parameter	Min. Value	Max. Value	Unit
Pressure	30	90	bar
Flow Rate	0.039	0.628	kg/s
Heat Flux	0.0	150.0	W/cm^2
Outlet Quality	8.0	80.0	%
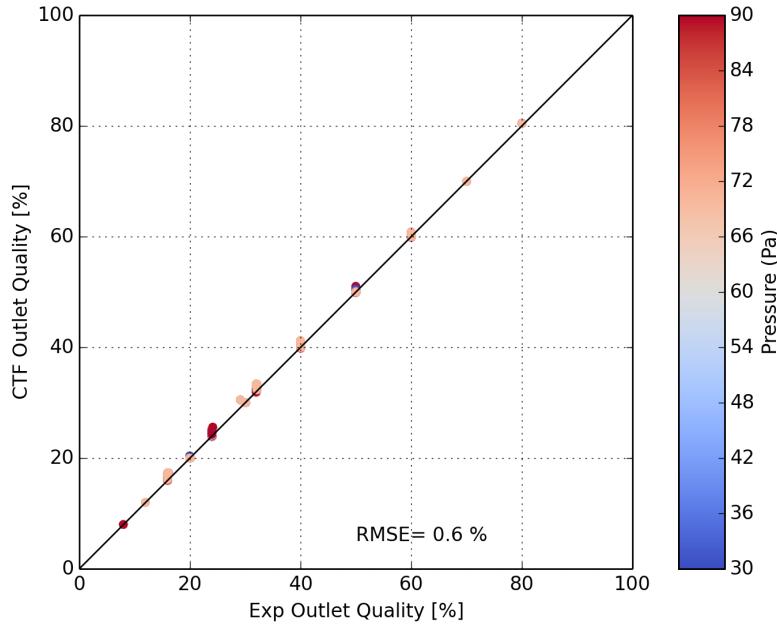
Figure 1. Comparison of CTF and experimental outlet quality.

The 9.0 m (354 in.) test section was divided into 320 uniformly-spaced axial nodes to give node sizes of roughly 1 in., which is consistent with the typically recommended mesh size for CTF calculations. A mesh sensitivity study was performed for Section 2.2 to verify that this nodalization was sufficiently spatially converged in terms of outlet flow fractions.

1.3   Entrainment Correlation

A brief review of the CTF entrainment model is provided in this section. CTF uses the Wurtz model [1], which was developed from the Riso test data. The Wurtz entrainment correlation is given by

$$S_E = \left(0.41\frac{\text{lbm}}{\text{ft}^2\text{s}}\right)\frac{k_s\tau_i\bar{U}_v\mu_l}{\sigma^2}, \tag{1}$$

and

$$S_{DE} = k_0C. \tag{2}$$

The physical terms in the model are given in the "Wurtz Analytical Model" section of Table 2. Definitions of all variables are given in Table 3.

Evidently, some physical parameters are modeled differently in CTF compared to the original prescription by Wurtz. These models are given in the "CTF" section of Table 2. Comparisons of calculated and measured values for some of these parameters are shown in Section 2.

Table 2. Expressions for Physical Parameter Models in the Entrainment and De-Entrainment Correlation

	Wurtz analytical model
Equivalent sand roughness	$k_s = 0.57\delta + 6625\text{ft}^{-1}\delta^2 - 3.56e6\text{ft}^{-2}\delta^3 + 1.5736e9\text{ft}^{-3}\delta^4$
Interfacial shear stress	$\tau_i = \left(\frac{dP}{dz}\right)_f \frac{r_{i2}}{2}$
Film thickness	δ calculated from Prandtl two-layer model
Mean vapor velocity	$\bar{U}_v$ calculated from Prandtl two-layer model
Mass transfer coefficient	$k_0 = \left(\frac{\text{m}}{\text{s}}\right) = \begin{cases} 3.0492e12\sigma^{5.3054} \\ 12.491\sigma^{0.8968} \end{cases}$
Droplet concentration	$C = \frac{\alpha_e \rho_l}{\alpha_e + \alpha_v}$

	CTF
Equivalent sand roughness	$k_s = 0.57\delta + 6625\text{ft}^{-1}\delta^2 - 3.56e6\text{ft}^{-2}\delta^3 + 1.5736e9\text{ft}^{-3}\delta^4$
Interfacial shear stress	$\tau_i = f_i \rho_v \bar{U}_{vl}$
Film thickness	$\delta = \frac{\alpha_l D_h}{4}$
Mean vapor velocity	$\bar{U}_v$ calculated from vapor field equations
Mass transfer coefficient	$k_0 = \left(\frac{\text{m}}{\text{s}}\right) = \begin{cases} 3.0492e12\sigma^{5.3054} \\ 12.491\sigma^{0.8968} \end{cases}$
Droplet concentration	$C = \frac{\alpha_e \rho_l}{\alpha_e + \alpha_v}$

Table 3. Nomenclature for Entrainment Correlations

Symbol	Definition
S_E	entrainment rate
S_{DE}	de-entrainment rate
k_s	equivalent sand roughness of the liquid film
τ_i	interfacial shear stress
$\bar{U}_v$	mean vapor velocity
μ_l	liquid viscosity
σ	surface tension
k_0	mass transfer coefficient from droplets to film
C	mean concentration of liquid droplets in the vapor region
δ	film thickness
$\left(\frac{dP}{dz}\right)_f$	frictional pressure gradient
r_{i2}	interfacial radius
f_i	interfacial friction factor
ρ_v	vapor density
$\bar{U}_{vl}$	velocity difference between the vapor and film fields
α_e	volume fraction of liquid droplets
α_v	volume fraction of vapor
α_l	volume fraction of liquid film
ρ_l	liquid density
D_h	hydraulic diameter

2 RESULTS

2.1 Comparison of Film and Droplet Flow Rates

A comparison of film and droplet flow rates (as a fraction of the total flow rate) between CTF and the experimental data is shown in Figures 2 and 3, respectively. In general, CTF tends to predict similar film and droplet flow fractions relative to the experimental data for cases with high outlet quality, but tends to over-predict the film flow fraction (and under-predict the droplet flow fraction) relative to the experimental data for cases with low outlet quality.

The plotting script was expanded to look at results sensitivity to other simulation and test conditions, including:

- predicted outlet flow regime,

- facility tube diameter,

- test mass flux,

- test outlet pressure, and

- test power.

The results show a clear trend with respect to the CTF predicted flow regime. Figure 4 shows the film fraction with respect to the predicted flow regime using colors – blue dots represent the churn-turbulent flow regime, whereas red dots represent the annular/mist flow regime. Cases predicted to be in the churn-turbulent flow regime are consistently less accurately predicted than cases that are predicted to be in the annular/mist flow regime. Figure 5 shows a similar trend for the droplet flow fraction, which leads to conclusions similar to those drawn for the film figure.

As discussed in [2], this inaccuracy likely stems from the way CTF calculates closure terms for the churn-turbulent flow regime. CTF does not have a separate set of closure terms for the churn-turbulent flow regime, but, rather, it performs a linear interpolation between the closure terms of small-bubble/slug and annular/mist regimes. The interfacial drag terms, being an order-of-magnitude or more different for these two types of regimes, can lead to very poor predictions of the closure terms when the actual flow regime is very close to annular-mist. The resulting interpolated values will be heavily weighted towards the larger interfacial drag of the small-bubble/slug regime due to the fact that linear interpolation is used.

No significant accuracy trend with respect to tube diameter, mass flux, outlet pressure, or power level (diabatic vs. adiabatic) was found. Figures 6, 7, 8, and 9 show the film flow rate comparison with respect to these other checked parameters.

To determine if CTF's prediction accuracy is acceptable, CTF predictions were compared to the results found in [3], where a similar validation study using the Riso data was performed with COBRAG. Figure 10 shows the droplet flow fraction predicted by COBRAG for the 200 Series tests (adiabatic tests performed in the 10 mm tube). The CTF results for the 200 Series tests were extracted and re-plotted to match the formatting of the COBRAG results and allow for a better comparison in Figure 11. Note that the droplet flow fraction in these figures is with respect to the total liquid flow rate rather than the total flow rate as in earlier plots. The two codes show similar behavior in terms of the droplet flow fraction. Table 4 demonstrates that mean and root-mean-square (RMS) errors are very similar for this data set.

2.2 CTF Numerical Convergence Study

Figure 12 shows the results of a sensitivity study that analyzed the number of uniformly spaced axial nodes in the CTF output. The mesh is well-converged in terms of the root-mean-square error (RMSE) of flow fractions versus experimental values when using 80 or 160 axial nodes; however, a small number of cases still gave a significant change in flow fractions up to 320 nodes and possibly beyond. To maintain reasonable runtimes while ensuring sufficient spatial convergence, 320 axial nodes were used for all remaining calculations in this report.
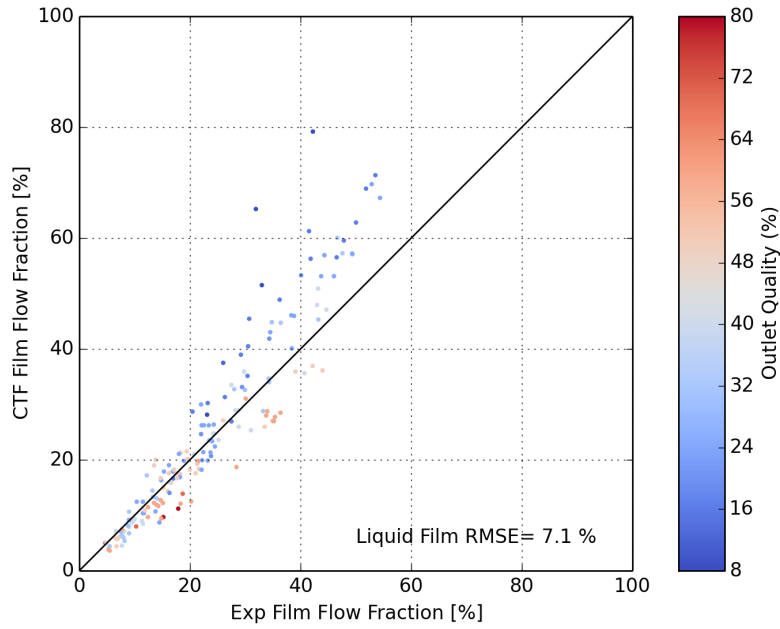
Figure 2. Comparison of CTF and experimental results for film flow rate at the outlet as a fraction of total flow.
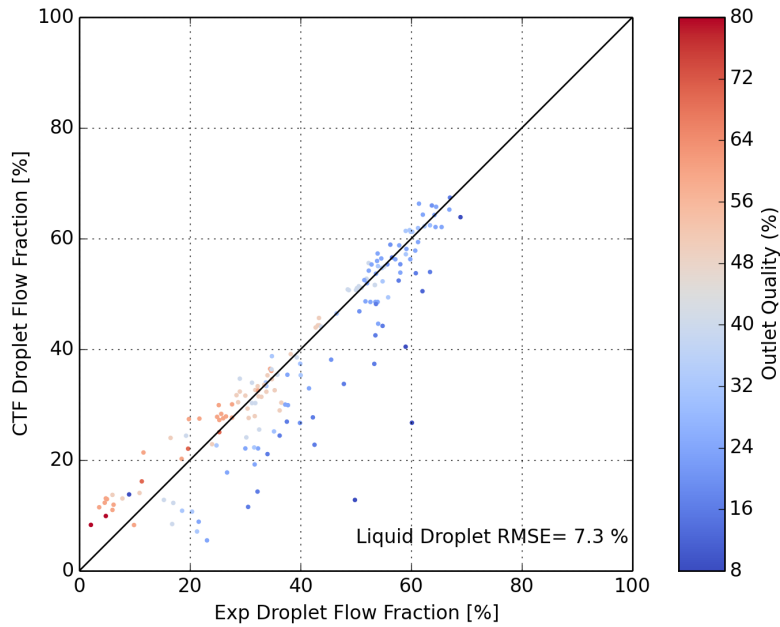
Figure 3. Comparison of CTF and experimental results for droplet flow rate at the outlet as a fraction of total flow.
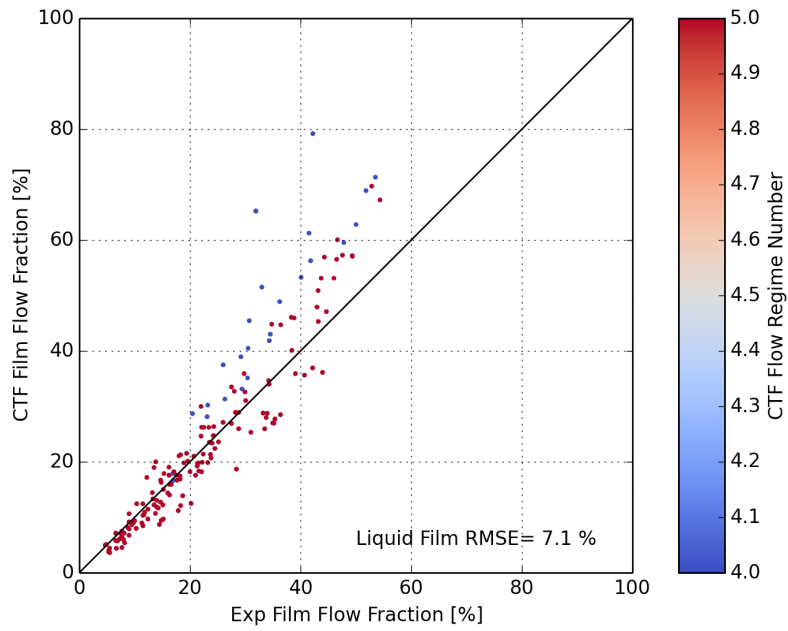
Figure 4. Sensitivity of film flow rate results to predicted flow regime (red denotes annular/mist, blue denotes churn-turbulent).
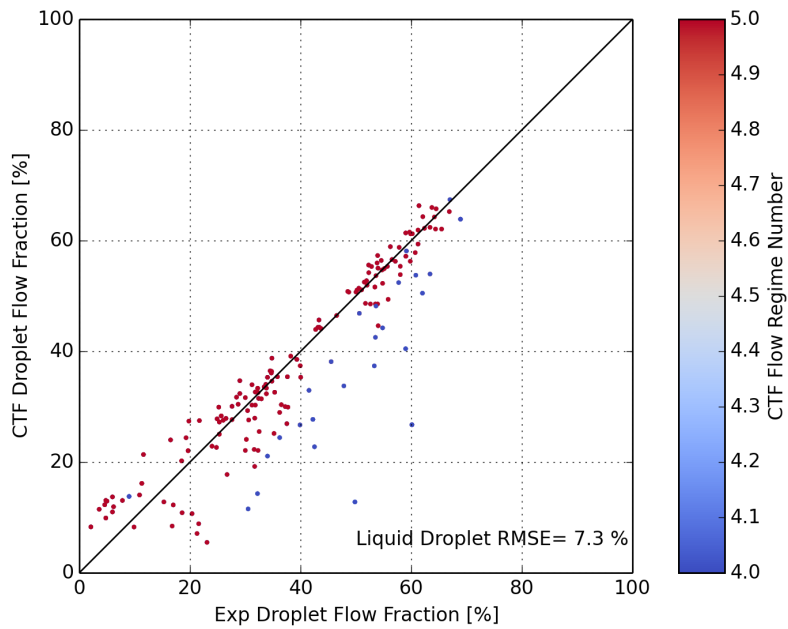
Figure 5. Sensitivity of droplet flow rate results to predicted flow regime (red denotes annular/mist, blue denotes churn-turbulent).
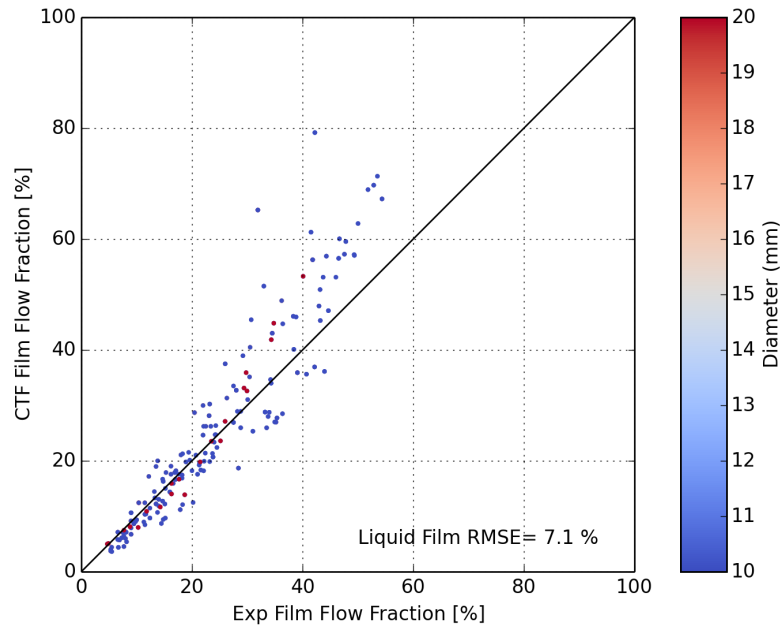
Figure 6. Sensitivity of film flow rate results to tube diameter.
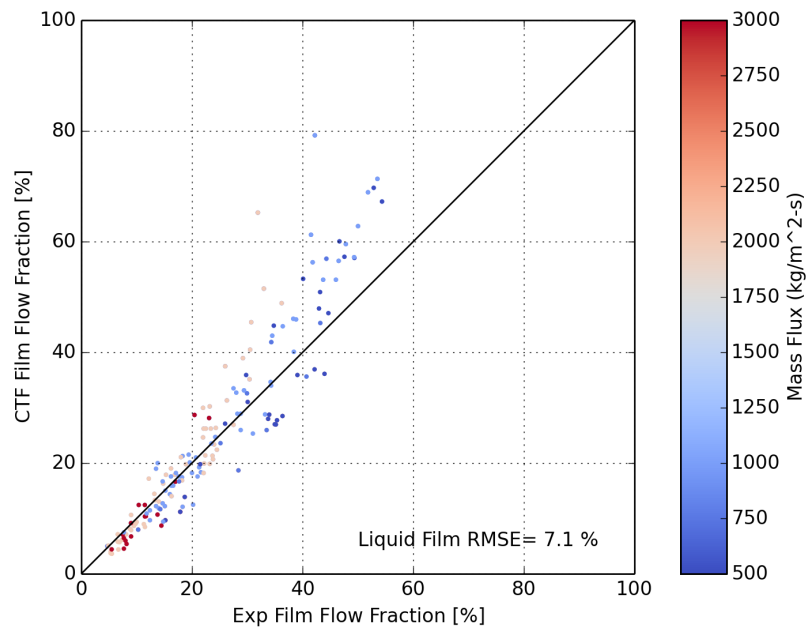
Figure 7. Sensitivity of film flow rate results to inlet mass flux.
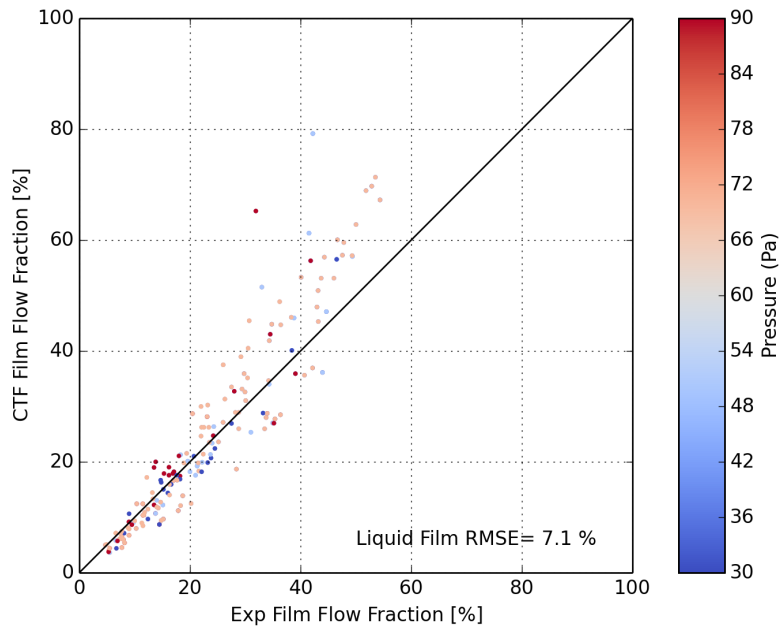
Figure 8. Sensitivity of film flow rate results to outlet pressure.
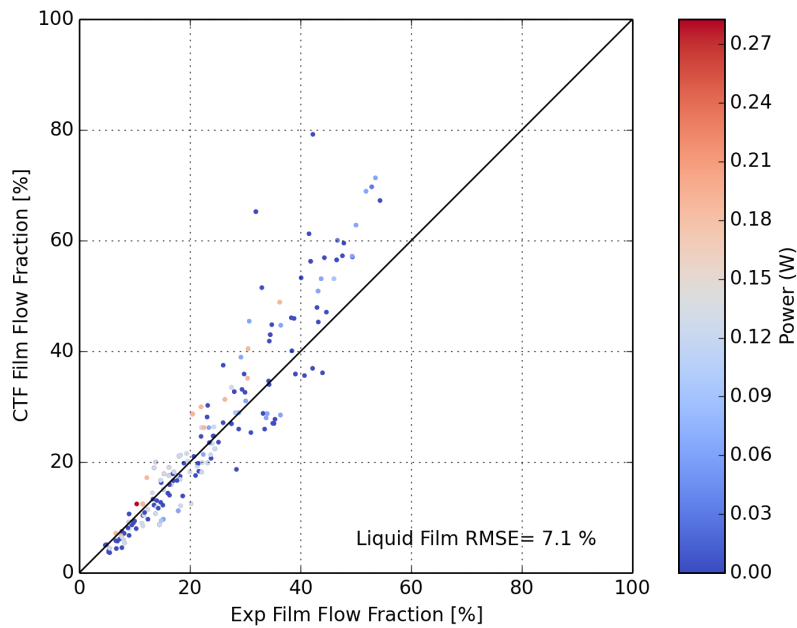
Figure 9. Sensitivity of film flow rate results to facility power (zero power refers to adiabatic cases).
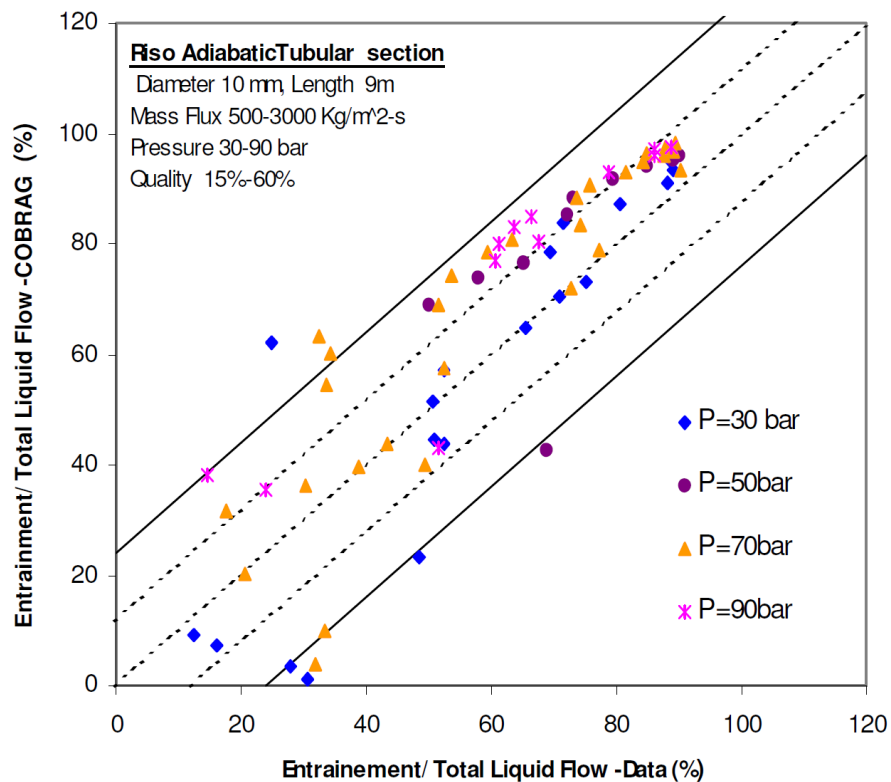
**Figure 10. COBRAG droplet flow fraction results for the adiabatic 10 mm pipe case
[3]**
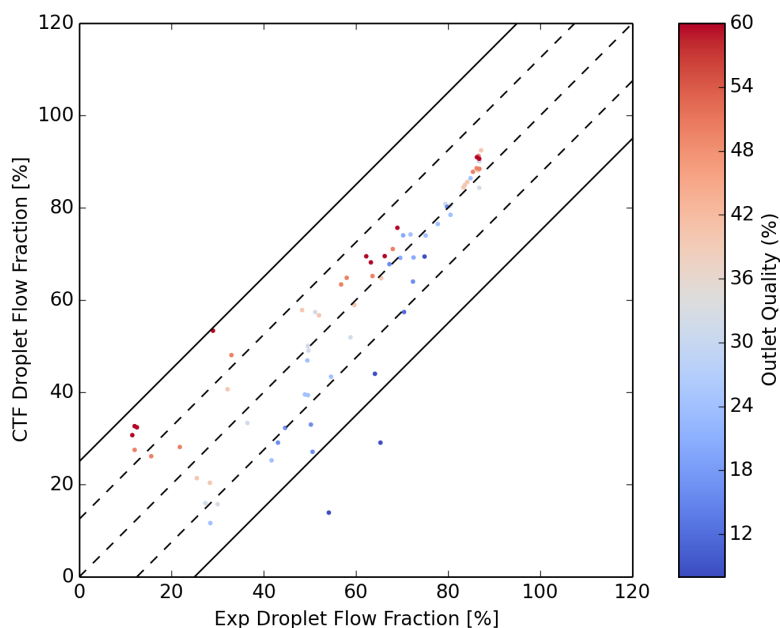
Figure 11. CTF droplet flow fraction results for the adiabatic 10 mm pipe case

Table 4. Droplet Flow Fraction Statistics for COBRAG and CTF for the 200 Series Riso Cases

Statistic	CTF	COBRAG
Mean Error	-1.0%	-1.7%
RMS	11.3 %	13.5 %
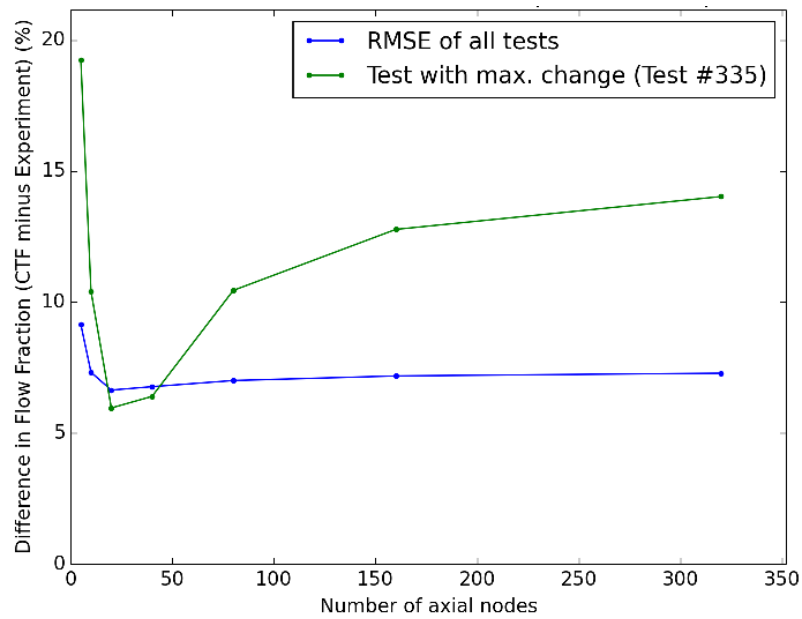
Figure 12. Difference in CTF versus experimental droplet flow fractions as a function of number of CTF axial nodes.

For each CTF run, to verify that the solution had converged in time and was not changing from iteration to iteration, all available convergence criteria for the normalized l_∞-norms of the CTF solution quantities were set to $1\cdot10^{-15}$; this ensured that the CTF solution reached the maximum iteration count (set to a large value of $2\cdot10^5$) to determine the asymptotic value achieved by each l_∞-norm convergence metric. A description of the l_∞-norm convergence criteria and their implementation is given in the CTF User Manual [4].

This calculation was performed for each of the 180 test cases. Table 5 shows a summary of the largest l_2- and l_∞-norm observed across all 180 cases, for each individual quantity captured in the convergence criteria. The overall maximum l_∞-norms for the liquid velocity field were witnessed in Case 367, which had an outlet void fraction of 92 % – one of the highest outlet void fractions among the 180 test cases. This coincides with previous studies [5], which have shown that CTF does not converge as tightly for high-void-fraction cases as it does for low-void-fraction cases.

Nevertheless, the highest l-norm for any variable is 0.0012 (in other words, 0.12 % of nominal values), which is sufficient convergence for this study because the experimental uncertainty in the Riso tests is considerably higher than this value, as was shown in Section 1.

2.3   Comparison to the Wurtz Model

Figures 13–17 show comparisons of the CTF-predicted film flow fraction values with Wurtz's experimental data and analytical calculations for the adiabatic test points. For almost all cases, the CTF predictions are in good agreement with the analytical model proposed by Wurtz, despite the differences noted in Table 2. Both the CTF results and the analytical model depart significantly from the experimental data for several of the test points with a low flow quality. This leads to the conclusion that the entrainment and de-entrainment models in CTF are implemented consistently with Wurtz' original model, and that differences between the CTF and experimental results are due primarily to deficiencies in the entrainment and de-entrainment correlations themselves, or possibly due to inaccuracies in the experimental data.

2.4   Pressure Drop Comparisons

Figure 18 shows a comparison of the drop in total pressure per unit length, across the top 1 m of the test section, between CTF and the experiment. Despite close agreement in flow quality, CTF predicts roughly three times the rate of pressure drop as was found in the experiment.

Considering that the Wurtz entrainment correlation includes dependence on both the rate of pressure drop and the film thickness, it is surprising that the CTF-predicted film and droplet flow fractions agree so closely with the Wurtz analytical calculations. To investigate further, the 200 Series data were extracted and re-plotted in Figure 19. The similar COBRAG results are shown in Figure 20. This additional comparison reveals that there is clearly a problem with the CTF modeling approach.

Table 5. Maximum Normalized l_2- and l_∞-norm Values across All Test Cases

| | l_2 | | l_∞ | |
	Max. Value	Index	Max. Value	Index
Void Fraction	$5.76\cdot10^{-7}$	379	$9.62\cdot10^{-6}$	379
Temperature	$6.70\cdot10^{-8}$	367	$8.39\cdot10^{-7}$	373
Pressure	$8.53\cdot10^{-6}$	367	$7.80\cdot10^{-5}$	367
Liquid Velocity	$1.11\cdot10^{-4}$	367	$1.23\cdot10^{-3}$	367
Vapor Velocity	$7.08\cdot10^{-6}$	367	$4.87\cdot10^{-5}$	367
Droplet Velocity	$2.78\cdot10^{-6}$	368	$9.42\cdot10^{-6}$	368

Figure 13. Comparison of film flow fractions between CTF, Wurtz' analytic calculations, and experimental results for the adiabatic test cases (P = 30 bar, d = 10 mm).

Figure 14. Comparison of film flow fractions between CTF, Wurtz' analytic calculations, and experimental results for the adiabatic test cases (P = 50 bar, d = 10 mm).

**Figure 15. Comparison of film flow fractions between CTF, Wurtz' analytic calculations,
and experimental results for the adiabatic test cases (P = 70 bar, d = 10 mm).**

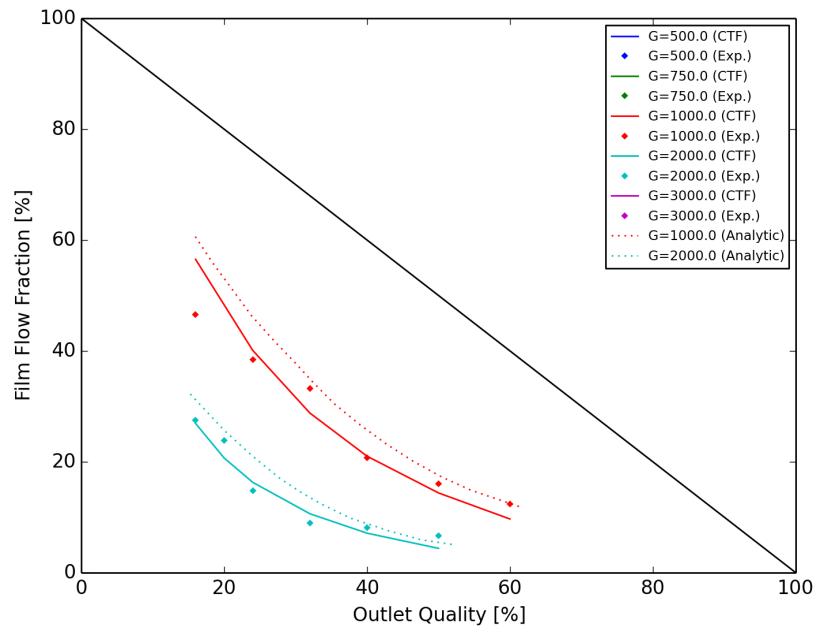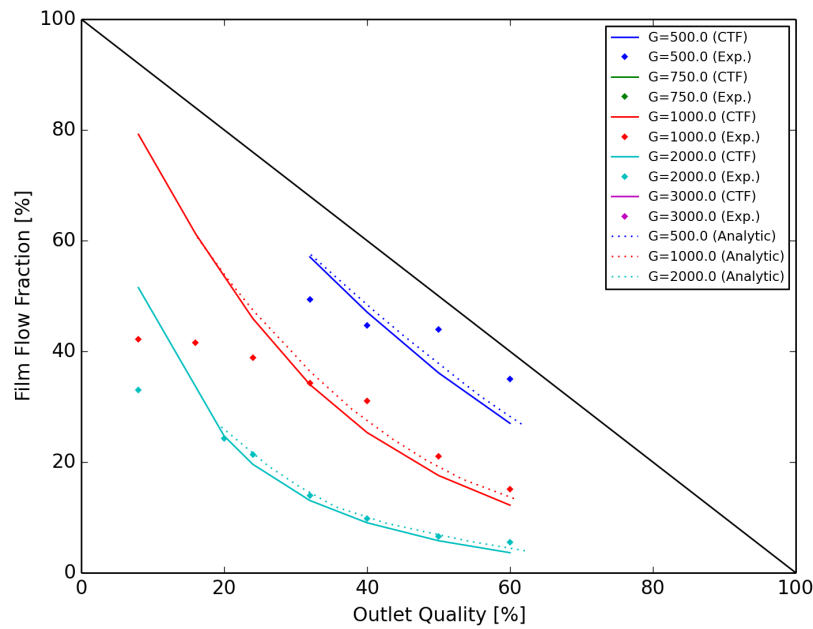**Figure 16. Comparison of film flow fractions between CTF, Wurtz' analytic calculations,
and experimental results for the adiabatic test cases (P = 90 bar, d = 10 mm).**

Figure 17. Comparison of film flow fractions between CTF, Wurtz' analytic calculations, and experimental results for the adiabatic test cases (P = 70 bar, d = 20 mm).

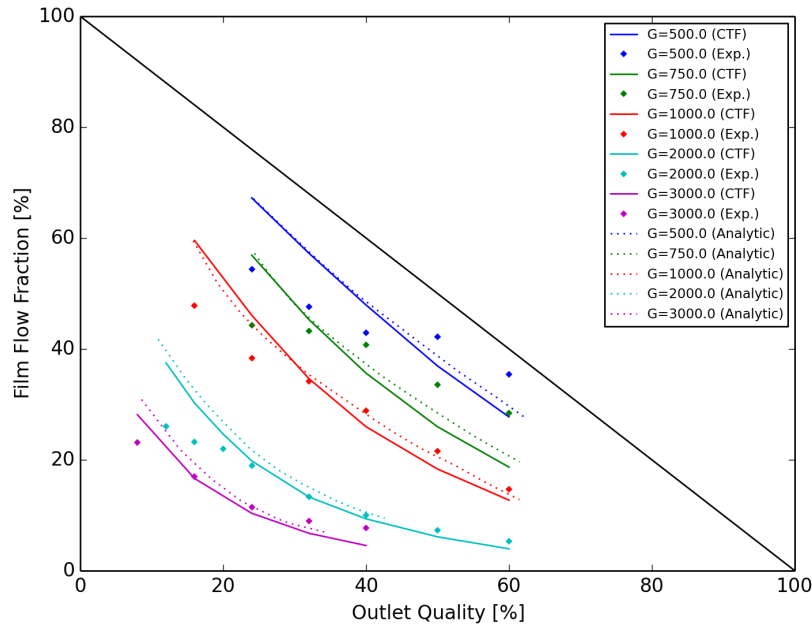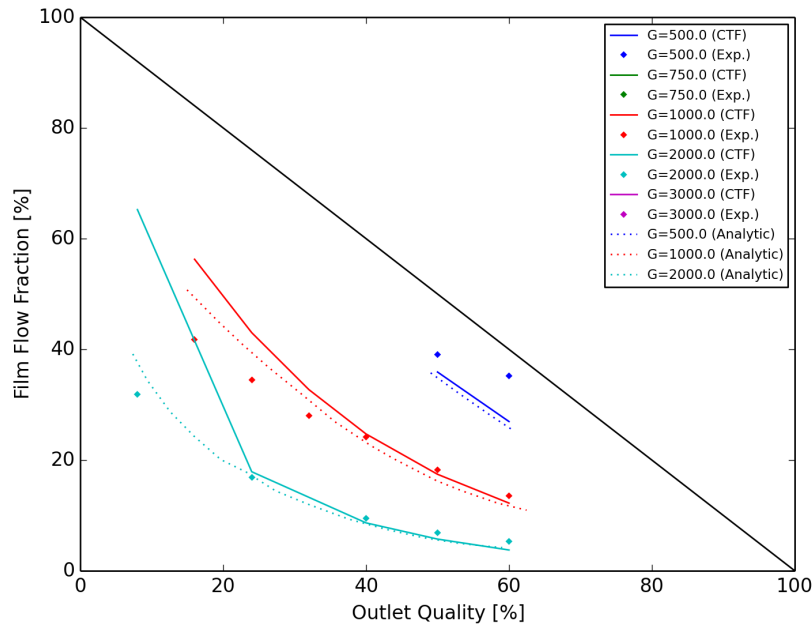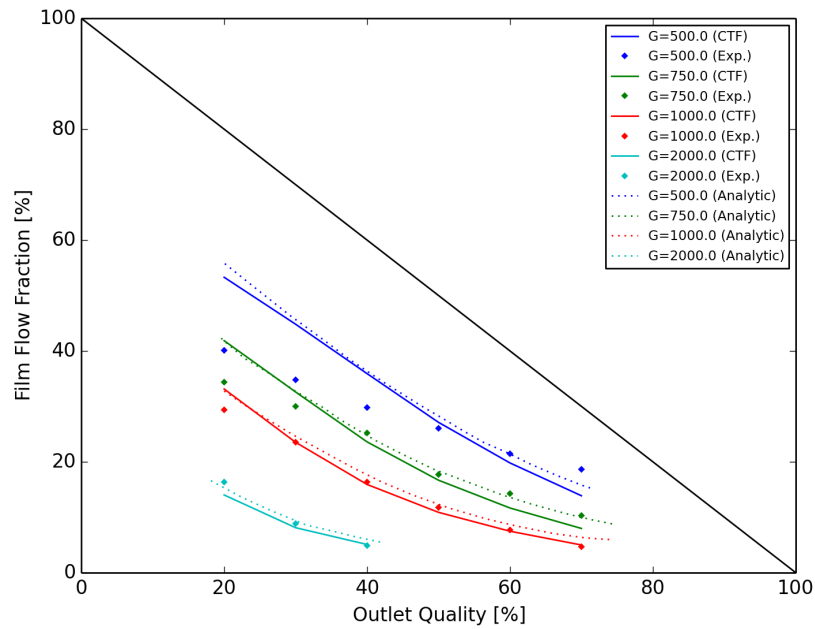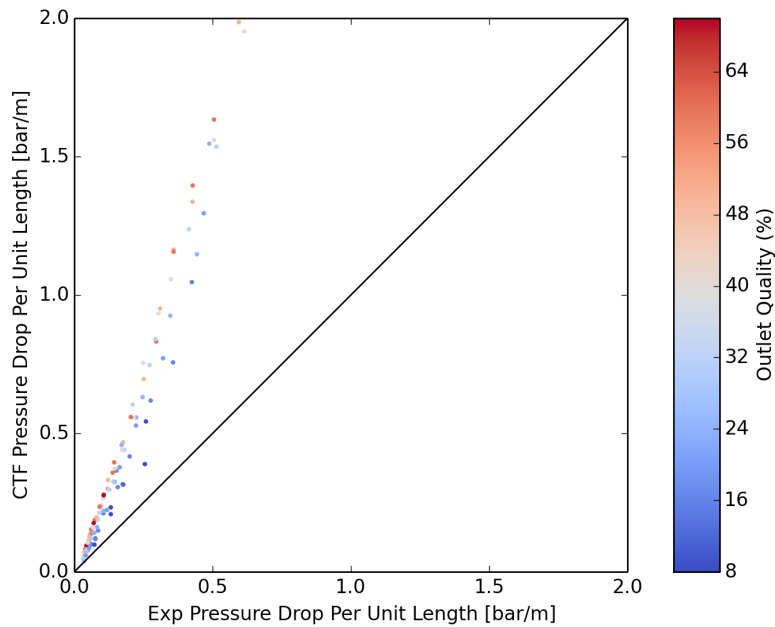**Figure 18. Measured vs. predicted total pressure drop per unit length at the outlet**
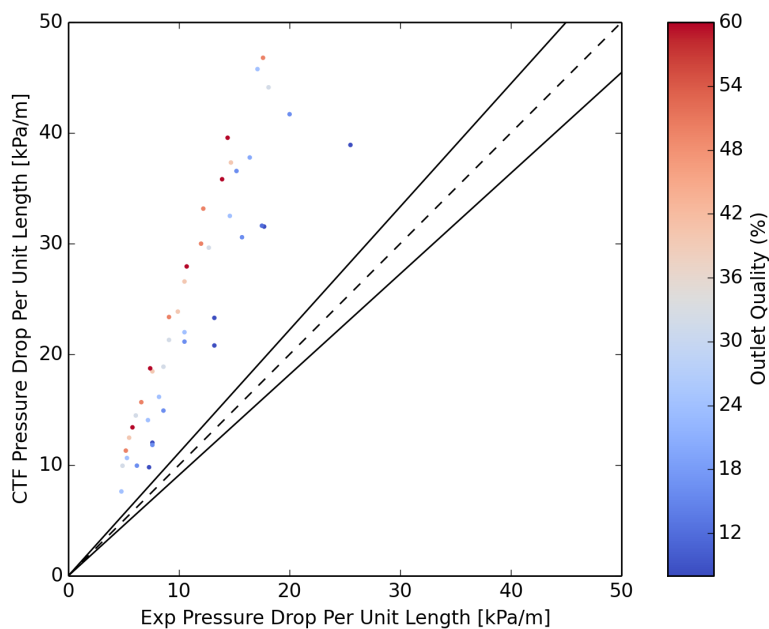
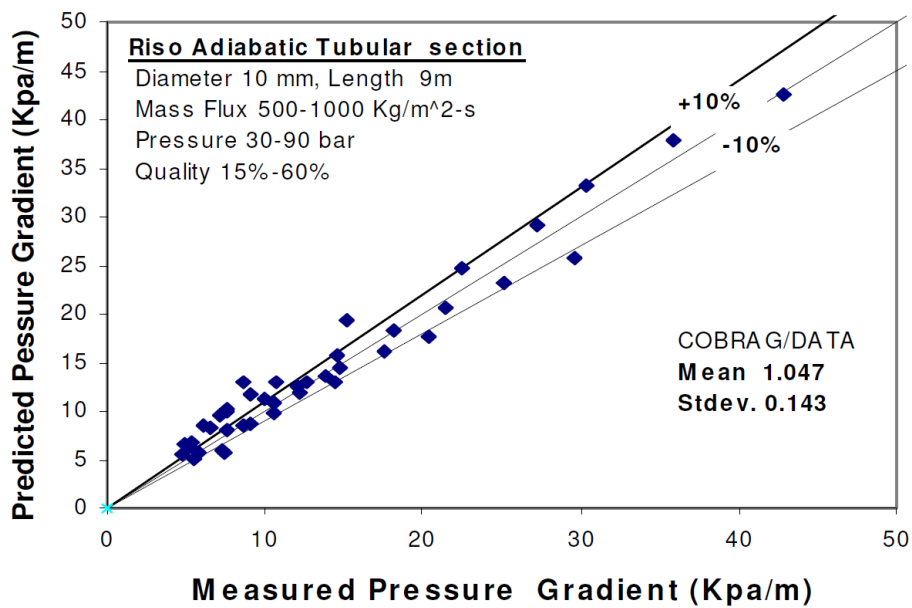**Figure 19. CTF pressure drop results for the adiabatic 10 mm pipe case**

Figure 20. COBRAG pressure drop results for the adiabatic 10 mm pipe case [3]

This revelation prompted a review of the CTF two-phase pressure drop model and interfacial drag model. The two-phase pressure drop model employs a two-phase multiplier as described by Wallis [6]; no discrepancies were found with the model as implemented in CTF. The interfacial drag is modeled using a two-region model; the Wallis interfacial drag model [6] is used for stable film flow, whereas the Henstock and Hanratty model [7] is used for unstable film flow. A significant deficiency in the implementation of the Henstock and Hanratty model was discovered as a result of the source code review. The Wallis model was disabled in the actual source code for unknown reasons, leaving the Henstock and Hanratty model to be used for all films, stable or unstable. This leads to a significant over-prediction of the interfacial drag and, thus, the two-phase pressure drop.

A simple test was performed whereby the Wallis model was used in place of the Henstock and Hanratty model for all Riso test cases. This led to a signficant improvement in two-phase pressure drop results, as shown in Figure 21. This test shows the high degree of sensitivity of the two-phase pressure drop predictions to the interfacial drag model employed. However, there is still a bias in the data even after switching the interfacial drag model. Also note that changing the interfacial drag model had no noticeable impact on the predicted film and droplet flow rates.

CTF is supposed to predict whether the film is stable or unstable by comparing the film void fraction to the critical void fraction as documented in the CTF Theory Manual [8], but this feature has been disabled in the code for unknown reasons. These deficiencies will be investigated and addressed in the future; however, as noted in [2], the annular/mist interfacial drag model that is described in the CTF Theory Manual may still lead to over-prediction of the two-phase pressure drop and may also suffer from numerical stability issues when the void fraction is close to the churn-turbulent, annular/mist transition point. This is because of the sharp discontinuity experienced in the closure term when the flow regime switches. With this in mind, it may be necessary to implement a more physically-correct model for treatment of this closure term.

2.5 Film Thickness Comparison

Figure 22 compares CTF's film thickness calculations to the experimental measurements of the 21 test points for which film thickness data was available. In general, CTF predicts a film thickness of roughly half that as measured in the experiments. The CTF results for the film flow fraction agree quite well with the experimental values for these cases, which means the film void fraction is being under-predicted by CTF. The film thickness is directly calculated the from film void fraction in CTF using a simple geometric relationship between film volume and film thickness (assuming the film is smooth and annular in shape). The film thickness discrepancy may be related to the discrepancy noted for the interfacial drag model. When the phase slip is inaccurate, as a result of the interfacial drag being inaccurate, the predicted film void fraction is affected. Significant inaccuracies in the combined liquid and droplet void fraction, if not addressed, will likely be problematic when CTF is ultimately used to provide thermal feedback to MPACT for annular/mist flow conditions.
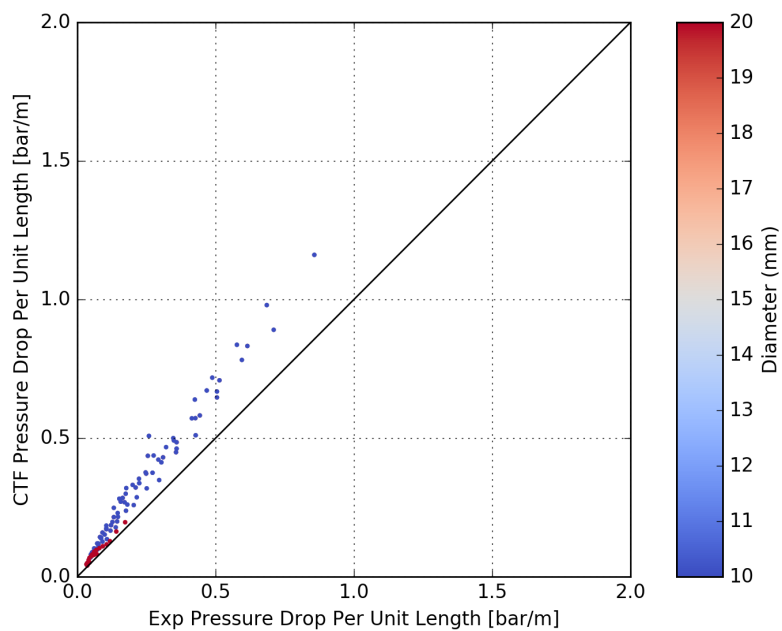
Figure 21. Predicted vs. experimental two-phase pressure drop when using the Wallis interfacial drag model only.
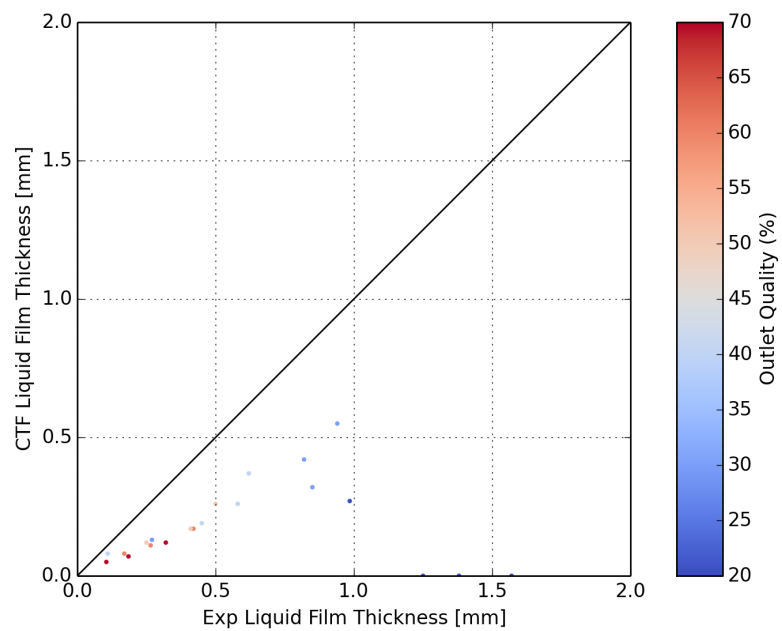
Figure 22. Measured vs. predicted outlet liquid film thickness

3   Conclusions

A set of 180 of the Riso flow experiments have been successfully modeled in CTF. The process of creating CTF input decks, extracting simulation data, and generating analysis plots has been completely automated, and all input files and scripts have been added to the COBRA-TF repository. Close agreement in film and droplet flow fractions was observed between CTF and the analytical clculations provided by Wurtz, except for cases with low flow quality. This agreement provided confidence that the entrainment models were implemented as intended, as the discrepancies between the calculated results and the experimental values were roughly on par with those seen by Wurtz. In other words, the poorer accuracy at low quality can be attributed to a deficiency in the entrainment model itself.

CTF showed reasonable agreement with similar COBRAG results in terms of droplet and film flow fraction. However, for the same cases, CTF showed a trend of substantially over-predicted two-phase pressure drop, prompting a review of the CTF two-phase friction and interfacial drag models. Deficiencies in the interfacial drag model were noted. This problem suggests that future resources should be devoted to further analysis of the annular/mist and churn-turbulent transition logic and models used for interfacial drag in those regimes, as prediction of behavior of the film layer will be important for accurate prediction of dryout in boiling water reactor conditions. It is also recommended that additional experimental data that measures entrainment and de-entrainment behavior in the annular/mist flow regime be added to the validation matrix in future studies.

Finally, future work should include adding CTF comparisons for some or all of the 55 tests involving annular flow geometry, as these tests might be more applicable to light water reactor fuel geometry and might yield further insights.

References

[1]   Jorgen Wurtz. *An Experimental and Theoretical Investigation of Annular Steam-Water Flow in Tubes and Annuli at 30 to 90 bar*. Tech. rep. Riso Report No. 372. Copenhagen, Denmark: Riso National Laboratory, Apr. 1978.

[2]   J. Lane. "The Development of a Comprehensive Annular Flow Modeling Package for Two-Phase Three-Field Transient Safety Analysis Codes". PhD thesis. The Pennsylvania State University, 2009.

[3]   B. Hizoum et al. "COBRAG Subchannel Analysis of BWR Fuel Thermal Hydraulic Performance". In *Proc. of 2010 LWR Fuel Performance/TopFuel/WRFPM*. Orlando, FL, USA, Sept. 2010.

[4]   R.K. Salko and M.N. Avramova. *CTF User Manual*. The Pennsylvania State University.

[5]   R. Salko et al. *CTF Void Drift Validation*. Tech. rep. CASL-U-2015-0320-002. Consrotium for Advanced Simulation of Light Water Reactors, 2015.

[6]   G.B. Wallis. *One-Dimensional Two-Phase Flow*. McGraw-Hill, 1969.

[7]   W.H. Henstock and T.J. Hanratty. "The Interfacial Drag and the Height of the Wall Layer in Annular Flows". In *AIChE Journal* 22.6 (1976), pp. 990–1000.

[8]   R.K. Salko and M.N. Avramova. *CTF Theory Manual*. The Pennsylvania State University.